Compression-Designs for Knowledge-Aided AMTI Radar Systems

Erlan H. Feria
The College of Staten Island (CSI) of the City University of New York (CUNY)
Department of Engineering Science and Physics
2800 Victory Blvd, Staten Island, New York, 10314
feria@mail.csi.cuny.edu

ABSTRACT

Compression ideas are applied to the design of exceedingly fast and lossy SAR imagery clutter covariance processors (CCPs) for use in knowledge-aided (KA) airborne moving target indicator (AMTI) radar subjected to severely taxing disturbances. Outstanding signal to interference plus noise ratio (SINR) radar performance is derived with a radar blind SAR imagery source coder that is characterized by its high compression, simplicity and universality. This result is surprising since it is found in a companion paper that radar blind schemes cannot be used with a 'lossless' straight CCP.

Keywords: Intelligent systems, radar, SAR imagery, prior knowledge, AMTI, source coding, processor coding, Compression Designs, Coding Designs, Conde

1. INTRODUCTION

A real-world problem whose high performance is attributed to its use of an intelligent system (IS) is knowledge-aided (KA) airborne moving target indicator (AMTI) radar such as found in DARPA's knowledge aided sensory signal processing expert reasoning (KASSPER) [1]. The IS consists of two subsystems in cascade. The first subsystem is a memory device containing the intelligence or prior knowledge. The intelligence is clutter whose knowledge facilitates the detection of a moving target. The clutter is available in the form of synthetic aperture radar (SAR) imagery where each SAR image requires 4MB of memory space. Since the required memory space for SAR imagery is prohibitive, it then becomes necessary to use 'lossy' memory space compression source coding schemes to address this problem. In [2] this problem was addressed with two distinct approaches. One approach was to design a simple and universal SAR imagery predictive-transform (PT) [3] compression scheme. This technique was radar blind since it did not make use of the antenna pattern and range bin geometry (APRBG). The other approach was to design a more complex radar seeing scheme. Of these two techniques only the radar seeing scheme was able to achieve outstanding signal to interference plus noise ratio (SINR) radar performance for a high compression ratio of 8,192. The second subsystem of the IS architecture is the intelligence processor (IP) which is a clutter covariance processor (CCP). The CCP is characterized by the on-line computation of a large number of complex matrices. A typical dimension for these matrices is 256 x 256 that results when both the number of antenna elements and transmitted antenna pulses during a coherent pulse interval (CPI) is 16. Clearly these computations significantly slow down the on-line derivation of the pre-requisite clutter covariances. In this paper these CCP computational issues are addressed using a novel 'processor coding' methodology [6] that inherently arises as the 'computational time compression dual' of Shannon's memory space compression source coding [7].

The processor coding methodology gives rise to an exceedingly fast clutter covariance processor compressor (CCPC). The CCPC consists of a look up memory containing a very small number of predicted clutter covariances (PCCs) that are suitably designed off-line using a small number of 'predicted' clutter powers (CPs) or PCPs and shifted antenna patterns (SAPs) where the SAPs are mathematical computational artifices not physically implemented. The on-line selection of the best PCC is achieved by investigating for each range bin the actual CP value as well as the clutter centroid (CC), which conveys information about the best SAP to select. It is shown in this paper that the proposed scheme yields outstanding SINR radar performance while in the presence of SAR imagery that has been either radar-blind or radar-seeing compressed by a factor of 8,192. This result is exceptional for two reasons. First, it demonstrates that the use of a highly 'lossy' and very fast CCPC can yield excellent SINR radar performance. Secondly, and just as

This work was supported in part by the Defense Advanced Research Projects Agency (DARPA) under the KASSPER Program Grant No. FA8750-04-1-004.

Mobile Multimedia/Image Processing for Military and Security Applications, edited by Sos S. Agaian, Sabah A. Jassim, Proc. of SPIE Vol. 6250, 625003, (2006) · 0277-786X/06/$15 · doi: 10.1117/12.669454

importantly, it shows that it serves as an 'enabler' of the radar blind SAR imagery compressor. This last result, in particular, is truly remarkable and its practical ramifications are further studied in [6]. Also in [6] it is established that the advanced CCPC can be viewed as a 'lossy processor coder' that is the computational time compression dual of a 'lossy source coder' [3]. Another observation of [6] is that the memory space compression source coding concepts of bit (or memory space needed to store a ***b***inary dig***it***), information (or minimum memory space needed to store a signal source outcome as measured by the logarithm of the reciprocal of its probability), and entropy (or average information associated with all possible signal source outcomes) have 'computational time compression processor coding duals' of bor (or time delay needed for the execution of some specified ***b***inary operat***or***), latency (or minimum time delay required to generate a scalar output for a signal processor after the internal structure of the signal processor has been redesigned subject to implementation components and architectural constraints), and ectropy (or maximum latency among all the latencies derived for the signal processor scalar outputs), respectively. Since both source coding and processor coding are compression based signals and systems design methodologies, their combination was given the name ***Co***mpressio***n-De***signs or ***Co***di***n***g-***De***signs (or Conde as is referred in short for either case reflecting a further compression) in [6]. In this paper the CCPC robustness is also studied and found to naturally lead to even faster CCPCs as well as to a SAP knowledge-aided sample matrix inverse (SMI) scheme. Finally in an appendix a novel PT sidelobe canceller for reduced-dimension adaptivity (RDA) [5] is offered.

The rest of this paper is organized as follows: In Section 2 the background material on KA-AMTI radar given in [2] is summarized to facilitate the reading of the current paper. In Section 3 the advanced CCPC is introduced and simulation results are discussed. In Section 4 a CCPC robustness study is made. In Section 5 conclusions are drawn.

2. BACKGROUND

2.1. The KA-AMTI Radar Problem

In Fig. 1 an overview of a KA-AMTI radar system is shown. It consists of two major structures. They are: 1) An iso-range ring, or range bin, for a uniform linear array (ULA) in uniform constant-velocity motion relative to the ground: only the front of the iso-range ring is shown corresponding to angle displacements from -90^o to 90^o relative to the antenna array boresight; and 2) An AMTI radar composed of an antenna, a space-time processor (STP) and a detection device. In KA-AMTI clutter returns are available in the form of SAR imagery that is obtained from a prior viewing of the area of interest. From this figure it is also noticed that the range bin is decomposed into N_C clutter cells. N_C is often greater than or equal to NM [4]-[5] where N is the number of antenna elements and M is the number of transmitted antenna pulses during a coherent pulse interval (CPI). In the simulations M = 16 and N=16 will be assumed. In Table 1 at the end of the paper a summary is given of all the simulations parameters including those for M and N.

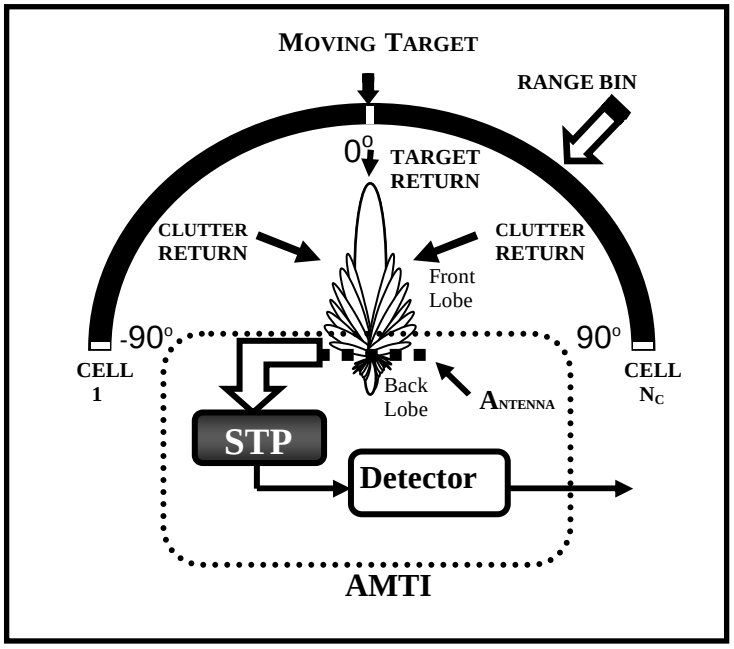

Fig. 1 The Overall Radar System

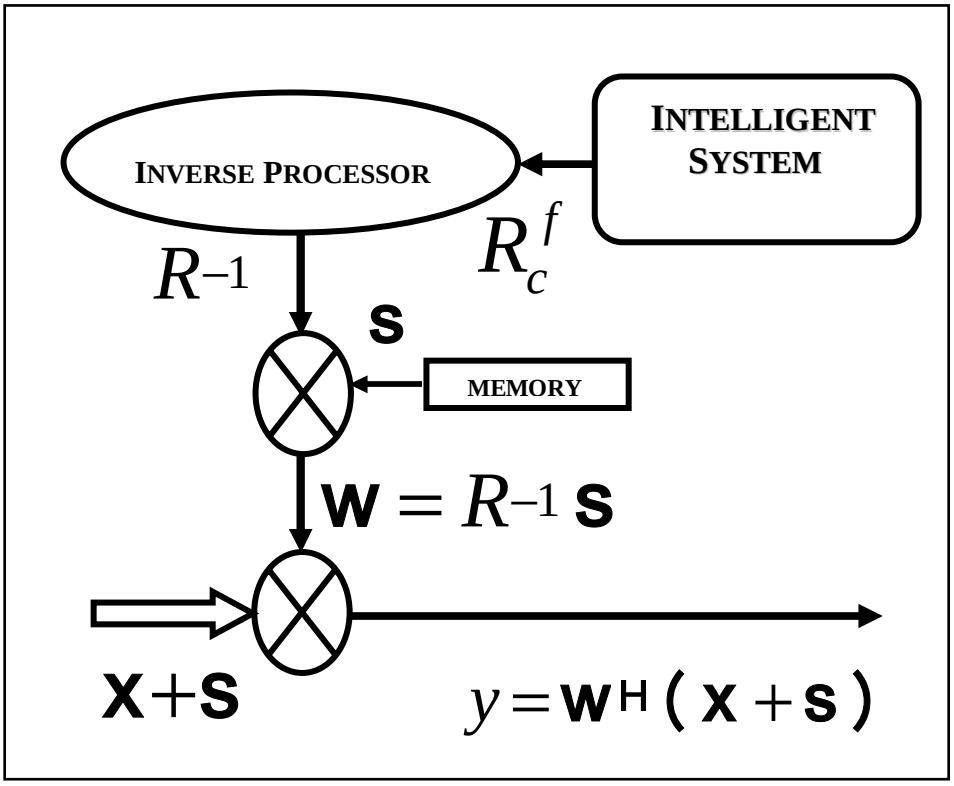

Fig. 2 The Space-Time Processor (STP)

Next the general architecture of the STP is shown in Fig. 2. From this system it is first noted that its input consists of the addition of two signals. They are:

1) The NM x 1 dimensional target steering vector **s** defined by

$$\mathbf{s} = [\underline{\mathbf{s}}_1(\theta_t)\ \underline{\mathbf{s}}_2(\theta_t) \ldots . \underline{\mathbf{s}}_M(\theta_t)]^H \tag{2.1}$$

$$\underline{\mathbf{s}}_k(\theta_t) = e^{j2\pi(k-1)\overline{f}_D^t}\underline{\mathbf{s}}_1(\theta_t) \quad for\ k = 1,\ldots,M \tag{2.2}$$

$$\underline{\mathbf{s}}_1(\theta_t) = [\mathrm{s}_{1,1}(\theta_t)\ \mathrm{s}_{2,1}(\theta_t)\ \ldots .\ \mathrm{s}_{N,1}(\theta_t)] \tag{2.3}$$

$$s_{k,1}(\theta_t) = e^{j2\pi(k-1)\overline{\theta}_t} \quad for\ k = 1,\ldots,N \tag{2.4}$$

$$\overline{f}_D^t = f_D^t / f_r \tag{2.5}$$

$$f_D^t = 2v_t / \lambda \tag{2.6}$$

$$f_r = 1/T_r \tag{2.7}$$

$$\overline{\theta}_t = \frac{d}{\lambda}\sin(\theta_t) \tag{2.8}$$

where: a) θ_t is the angle of attack (AoA) of the target with respect to boresight ; b) d is the antenna inter-element spacing; c) λ is the operating wavelength; d) $\overline{\theta}_t$ is the normalized θ_t; e) T_r is the pulse repetition interval (PRI); f) f_r is the pulse repetition frequency (PRF); g) v_t is the target radial velocity; h) f_D^t is the Doppler of the target; and i) $\overline{f}_D^t$ is the normalized f_D^t.

2) The NM x 1 dimensional vector **x** representing all system disturbances, which include the incident clutter, jammer, channel mismatch (CM), internal clutter motion (ICM), range walk (RW), antenna array misalignment (AAM), and thermal white noise (WN).

The NM x1 dimensional weight vector **w**, also shown in Fig. 2, multiplies the STP input **s**+**x** yielding the STP generally complex scalar output $y = \mathbf{w}^H(\mathbf{s}+\mathbf{x})$. The expression for **w** is in turn given by the direct inverse relation

$$\mathbf{w} = R^{-1}\mathbf{s} \tag{2.9}$$

that results from the maximization of the signal to interference plus noise ratio (SINR) [5]

$$\text{SINR} = \mathbf{w}^H\mathbf{s}\mathbf{s}^H\mathbf{w} / \mathbf{w}^H R\mathbf{w} \tag{2.10}$$

where the NM x NM dimensional matrix, R, is the total disturbance covariance defined by $R = E[\mathbf{x}\mathbf{x}^H]$. To model this covariance the covariance matrix tapers (CMTs) formulation of [5] was used resulting in

$$R = \{R_C \;\; O \;\; (R_{RW} + R_{ICM} + R_{CM})\} + \{R_J \;\; O \;\; R_{CM}\} + R_n \tag{2.11}$$

$$R_C = R_c^f + R_c^b \tag{2.12}$$

where R_n, R_c^f, R_c^b, R_C, R_J, R_{RW}, R_{ICM} and R_{CM} are covariance matrices of dimension NM x NM and the symbol O denotes a Hadamard product or element by element multiplication. Moreover these disturbance covariances correspond to: R_n to thermal white noise; R_c^f to front clutter; R_c^b to back clutter; R_C to total clutter; R_J to jammer; R_{RW} to range walk; R_{ICM} to internal clutter motion ; and R_{CM} to channel mismatch. In [5] the covariances R_{RW}, R_{ICM} and R_{CM} are referred as CMTs. All of these covariances are defined in the companion paper [2]. However, since in subsequent discussions the covariances R_n and R_c^f are repeatedly used, their definitions are given next:

Thermal white noise: R_n is defined as follows

$$R_n = \sigma_n^2 I_{NM} \tag{2.13}$$

where σ_n^2 is the average power of thermal white noise and I_{NM} is an identity matrix of dimension NM x NM. Notice from Table 1 that this noise power is assumed to be 1 in all simulations.

Front Clutter Covariance: R_c^f is the output of the intelligent system of Fig. 2 and is defined by

$$R_c^f = \sum_{i=1}^{N_C} p_c^f(\theta_c^i, \theta_t)\, \mathrm{c}^f(\theta_c^i, \theta_{AAM})\, \mathrm{c}^f(\theta_c^i, \theta_{AAM})^H \tag{2.14}$$

$$p_c^f(\theta_c^i, \theta_t) = G_A^f(\theta_c^i, \theta_t)\; {}_f\sigma_{c,i}^2 \tag{2.15}$$

$$G_A^f(\theta_c^i, \theta_t) = K^f \left| \sin\left\{ N\pi \frac{d}{\lambda}(\sin(\theta_c^i) - \sin(\theta_t)) \right\} / \sin\left\{ \pi \frac{d}{\lambda}(\sin(\theta_c^i) - \sin(\theta_t)) \right\} \right|^2 \tag{2.16}$$

$$\mathrm{c}^f(\theta_c^i, \theta_{AAM}) = [{}_f\underline{c}_1(\theta_c^i, \theta_{AAM}) \;\; {}_f\underline{c}_2(\theta_c^i, \theta_{AAM}) \ldots\ {}_f\underline{c}_M(\theta_c^i, \theta_{AAM})]^H \tag{2.17}$$

$${}_f\underline{c}_k(\theta_c^i, \theta_{AAM}) = e^{j2\pi(k-1)\bar{f}_D^{c_f}(\theta_c^i, \theta_{AAM})}\, \underline{c}_1(\theta_c^i) \tag{2.18}$$

$$\text{for } k = 1, \ldots, M$$

$$\underline{c}_1(\theta_c^i) = [c_{1,1}(\theta_c^i) \;\; c_{2,1}(\theta_c^i) \;\ldots\; c_{N,1}(\theta_c^i)] \tag{2.19}$$

$$c_{k,1}(\theta_c^i) = e^{j2\pi(k-1)\bar{\theta}_c^i} \quad \text{for } k = 1, \ldots, N \tag{2.20}$$

$$\bar{f}_D^{c_f}(\theta_c^i, \theta_{AAM}) = \beta\bar{\theta}_c^i \{\cos(\theta_{AAM}) + \sqrt{\sin^2(\theta_{AAM}) + (\cos^2(\theta_{AAM}) - 1)\sin^2(\theta_c^i)}\,/\sin(\theta_c^i)\} \tag{2.21}$$

$$\beta = \frac{v_p T_r}{d/2} \tag{2.22}$$

$$\bar{\theta}_c^{\,i} = \frac{d}{\lambda}\sin(\theta_c^i) \tag{2.23}$$

where: a) the index i refers to the i[th] front clutter cell on the range bin section shown on Fig. 1; b) θ_c^i is the AoA of the i[th] clutter cell; c) θ_{AAM} is the antenna array misalignment angle [5]; d) ${}_f\sigma_{c,i}^2$ is the i[th] front clutter source cell power (excluding the antenna gain); e) $G_A^f(\theta_c^i,\theta_t)$ is the antenna pattern gain associated with the i[th] front clutter cell; f) K^f is the front global antenna gain; g) $p_c^f(\theta_c^i,\theta_t)$ is the "total" i[th] front clutter cell power (in the simulations the 4 MBs SAR image of the Mojave Airport in California of Fig. 3 is used [1] where: i) this figure depicts the resolution clutter source cell power in dBs; ii) the down range is 1500 meters represented by 1024 rows; and iii) the cross range is 1800 meters represented by 256 columns. In addition, groups of sixteen consecutive rows are averaged to yield the 64 range bins depicted in Fig. 4. Moreover Fig. 5 presents the front clutter power (CP), i.e.,

$$CP = R_c^f(1,1) = \sum_{i=1}^{N_C} p_c^f(\theta_c^i,\theta_t), \tag{2.24}$$

for the 64 range bins with values ranging from 41 to 75 dBs); h) $c^f(\theta_c^i,\theta_{AAM})$ is the NM x 1 dimensional and complex i[th] clutter cell steering vector; i) v_p is the radar platform speed; j) $\bar{\theta}_c^{\,i}$ is the normalized θ_c^i; and k) β is the ratio of the distance traversed by the radar platform during the PRI, v_pT_r, to the half antenna inter-element distance, d/2.

At this point it should be noted that expressions (2.14)-(2.15) define the clutter covariance processor or intelligence processor of the intelligent system of Fig. 2. In addition, the front clutter source cell power ${}_f\sigma_{c,i}^2$ is the output of the intelligence source that the intelligence processor operates on.

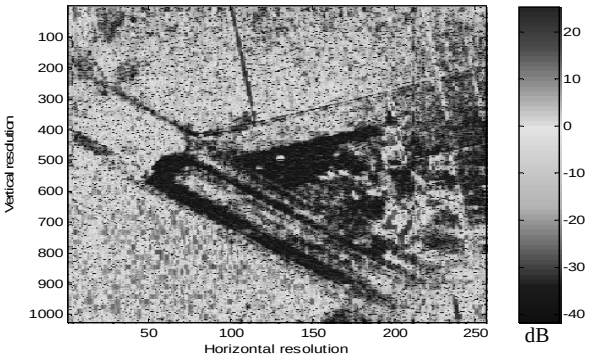

Fig. 3 1024 x 256 4MB SAR

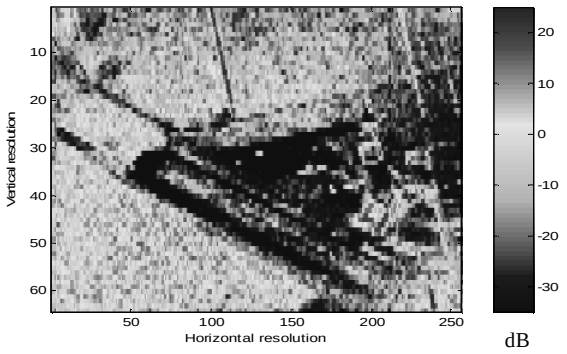

Fig. 4 64 Range Bins of SAR Image

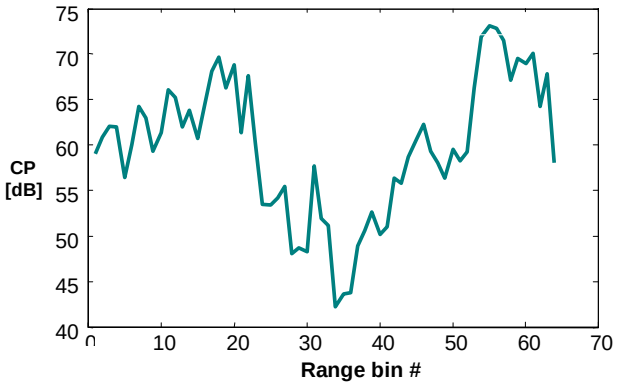

Fig. 5 CP vs Range Bin #

2.2. Radar Blind and Radar Seeing Source-Coders

In this subsection the radar blind and radar seeing source coders advanced in the companion paper [2] are reviewed. The discussion begins with Fig. 6 which presents the intelligence source and intelligence processor subsystems of the intelligent system of Fig. 2. The intelligence source contains the stored SAR imagery or clutter while the intelligence-processor or CCP uses as its external input the output of the SAR imagery source, and as internal inputs the antenna pattern and range bin geometry or APRBG and the front clutter steering vectors (2.17) to compute the front clutter covariance matrix (2.14). Although this system produces optimum SINR radar performance it is highly

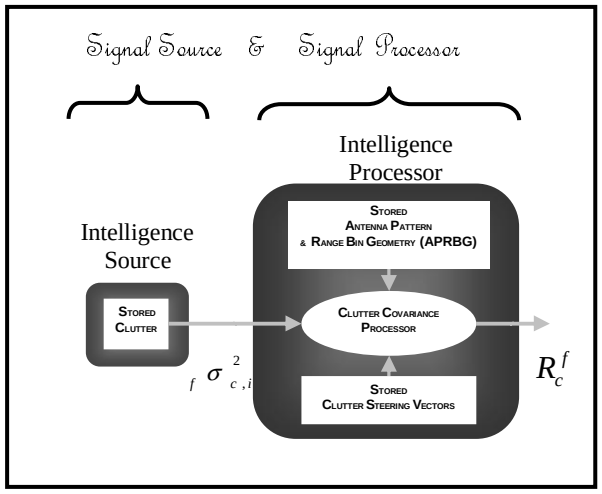

Fig. 6 Intelligent System

inefficient in terms of both its memory storage and on-line computing hardware requirements. To alleviate the memory storage problem associated with the intelligent system two different types of source coders were investigated in [2] as tentative replacements for the intelligence-source of Fig. 6. These were a simple predictive-transform (PT) [3] radar-blind scheme that is oblivious to the APRBG and a more elaborate radar-seeing scheme that makes use of the APRBG. These two schemes are now reviewed in the form of block diagram descriptions.

2.2.1. Radar-Blind Clutter Coder (RBCC): In Fig. 7 the basic structure of a radar-blind clutter coder (RBCC) is presented. It is an intelligence source coder containing the compressed or encoded clutter where the APRBG was not used when designing it. The obvious advantage of a radar-blind clutter coder is that the compressed clutter can be used with any kind of AMTI radar system without regard to the actual APRBG environment. A clutter decompressor is also necessary in order to derive an estimate for the uncompressed clutter for use by the straight CCP or intelligence processor. The combination of the RBCC and straight CCP is denoted here as RBCC-CCP for short. In the companion paper [2] it was found that this simple scheme did not produce a satisfactory SINR radar performance with reasonable compression ratios for SAR imagery.

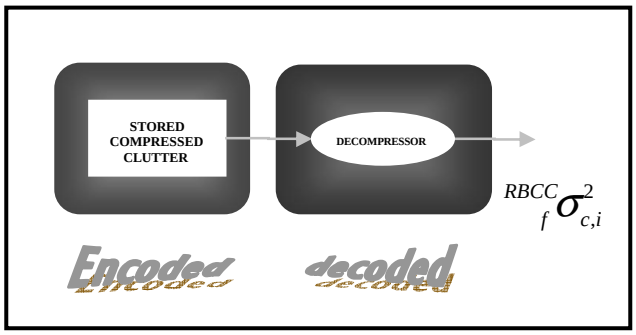

Fig. 7 Radar-Blind Clutter Coder (RBCC)

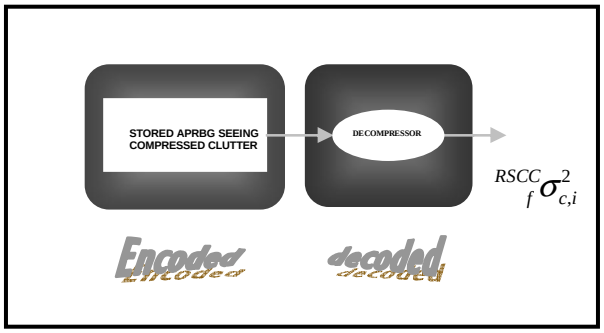

Fig. 8 Radar-Seeing Clutter Coder (RSCC)

2.2.2. Radar-Seeing Clutter Coder (RSCC): In Fig. 8 the radar-seeing clutter coder (RSCC) structure is shown where the only difference from that of the radar-blind case of Fig. 7 is that the source-coder makes use of the APRBG. The combination of the RSCC and a straight CCP is denoted as RSCC-CCP for short. In the companion paper [2] it is shown that outstanding SINR radar performance is derived when SAR imagery is compressed from 4 MB to 512 bytes for a compression ratio of 8,192.

3. THE CLUTTER COVARIANCE PROCESSOR COMPRESSOR

In this section a clutter covariance processor compressor (CCPC) is advanced that achieves significant 'on-line' computational time compression of the straight clutter covariance processor or CCP. In [6] it is shown that the CCPC can be viewed as the computational time compression dual of a 'lossy' source coder. The proposed CCPC is eminently lossy since its output does not emulate that of the straight CCP. This is the case since its stated objective is to derive outstanding SINR radar performance regardless of how well its output compares with that of the local intelligence processor. The discussion starts by first noticing that the computational burden or time delay of the straight CCP describing equations (2.14)-(2.15) is governed by the need to determine "on-line" the front clutter steering matrix $c^f(\theta_c^i,\theta_A)c^f(\theta_c^i,\theta_A)^H$ N_c times, where each of these NM x NM dimensional matrices is weighted by the scalar and real

cell power $p_c^f(\theta_c^i,\theta_t)$. Furthermore, from expression (2.15) it is noted that the shape of the range bin cell power is a function of the antenna pattern $G_A^f(\theta_c^i,\theta_t)$ as well as the front clutter source cell power ${}_f\sigma_{c,i}^2$ which often varies drastically from range bin to range bin. Clearly the variation of the clutter source cell power ${}_f\sigma_{c,i}^2$ from range bin to range bin is the source of the on-line computational burden associated with (2.14)-(2.15) since otherwise these expressions could have been solved off-line.

Next the on-line computational time delay problem of the straight CCP is addressed in two steps where each step has two parts.

STEP I:

Part I.A *External CCP Input:* In this first part a simple mathematical model for the external input of the CCP is sought. This external input is the clutter source cell power waveform $\{ {}_f\sigma_{c,i}^2 \}$ and its mathematical model is selected to be the power series

$$K_0+K_1 i+K_2 i^2+\ldots, \tag{3.1}$$

where K_j for all j are real constants that are determined on-line for each range bin using as a basis the measured input waveform $\{ {}_f\sigma_{c,i}^2 \}$. Since our objective is to achieve the smallest possible "on-line" computational time delay while yielding a satisfactory SINR radar performance, a single constant, K_0, has been selected to model the entire clutter source cell power waveform. The numerical value for K_0 will depend on the strength of the clutter and its centroid (to be discussed in Part I.B). The strength of the clutter is related to the front clutter power CP defined earlier in (2.24) and plotted in Fig. 5 for the 64 range bins of Fig. 4. The CP will be one of two real and scalar values derived 'on-line' by the CCPC.

Part I.B *Internal CCP Input:* In this second and last part of Step I a suitable modulation of the antenna pattern waveform $\{ G_A^f(\theta_c^i,\theta_t) \}$ is sought. The modulation of this internal CCP input can be achieved in several ways. Two of them are: a) By using peak-modulation which consists of shifting the peak of the antenna pattern to some direction away from the target; and b) By using antenna elements-modulation which consists of widening or narrowing the antenna pattern mainbeam by modifying the number of "assumed" antenna elements N. It is emphasized here that what is being proposed is only a mathematical alteration of the antenna pattern since the true antenna pattern remains unaffected. Peak-modulation has been selected since, as mentioned earlier, the main objective is to achieve the smallest possible "on-line" computational delay for the computational time compressed CCP. Furthermore, to guide us in finding the position to where the peak of the antenna pattern should be shifted to, the clutter centroid (CC) or center of mass of the clutter is evaluated for each range bin. The CC is the second of two scalar values evaluate on-line by the CCPC and is given by the following expression

$$CC = \sum_{i=1}^{N_C} i\ p_c^f(\theta_c^i,\theta_t)/CP\,. \tag{3.2}$$

In Fig. 9 the CC plot is shown for the 64 range bins of the SAR image given in Fig. 4. Note that for many of the 64 range bins the CC varies significantly from the position of the assumed target at 128.5 (0^o from boresight). Clearly for the isotropic clutter case the CC will reside at boresight.

STEP II

Part II.A *Off-Line Evaluations:* In this first part of Step II a finite and fixed number of predicted clutter covariances or PCCs are found off-line. This is done using the CCP describing equations (2.14)-(2.15) subject to the simple clutter model (3.1) and a modulated antenna pattern which results in a small and fixed number of highly lossy clutter covariance realizations. The PCCs are derived from the following expressions:

$$PCC(k,j)=\sum_{i=1}^{N_C} p_{pc}^f(\theta_c^i,\theta_t,\theta^k,PCP_j)c^f(\theta_c^i,\theta_A)c^f(\theta_c^i,\theta_A)^H \tag{3.3}$$

$$k=1,\ldots,N_{SAP} \quad \& \quad j=1,\ldots,N_{PCP}$$

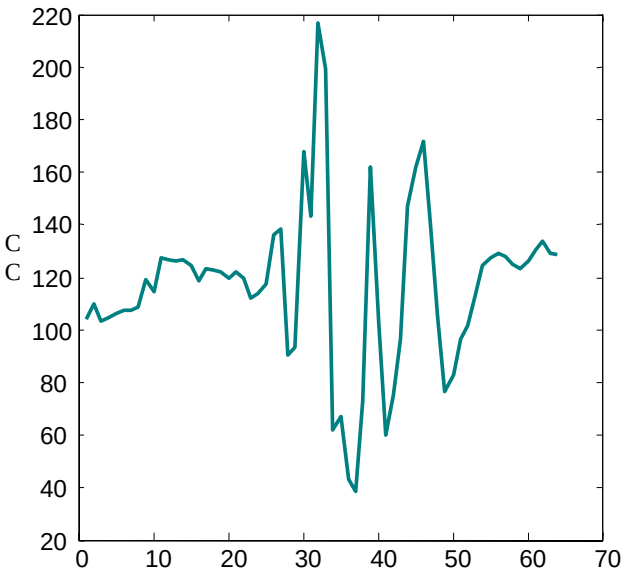

Fig. 9 CC versus Range Bin #

$$p_{pc}^{f}(\theta_c^i, \theta_t, \theta^k, PCP_j) = K_0(PCP_j, \theta^k) G_A^f(\theta_c^i - \theta^k, \theta_t) \quad (3.4)$$

$$PCP_j = K_0(PCP_j, \theta^k) \sum_{i=1}^{N_C} G_A^f(\theta_c^i - \theta^k, \theta_t) \quad (3.5)$$

$$PCP_j \in [PCP_{Min}, ..., PCP_{Max}] \quad (3.5a)$$

where: a) $p_{pc}^{f}(.)$ is the predicted front clutter power; b) $G_A^f(\theta_c^i - \theta^k, \theta_t)$ is a shifted antenna pattern or SAP where the peak value of the actual antenna pattern (2.16) has been shifted from $\theta_c^i = \theta_t$ to $\theta_c^i = \theta_t + \theta^k$; c) θ^k denotes the amount of angular shift of the SAP away from the assumed target position θ_t (the SAPs are generally designed in pairs, one associated with θ^k and the other with - θ^k); d) N_{SAP} is the number of SAPs considered (in the simulations the cases with N_{SAP} = 1, 3 and 5 will be studied); e) PCP_j is the j[th] predicted CP or PCP value; e) $K_0(PCP_j, \theta^k)$ is the PCC constant gain that together with $G_A^f(\theta_c^i - \theta^k, \theta_t)$ gives rise to PCP_j from (3.5); f) N_{PCP} is the number of assumed PCP values (in the simulations N_{PCP} = 2); and f) PCP_{Min} and PCP_{Max} are minimum and maximum PCP values, respectively, suitably evaluated for each SAR image (assumed to be 57 and 75 dBs for the SAR image investigated).

Part II.B *On-Line Evaluations:* In this last part of Step II the predicted intelligence processor output, or PCC, that better matches the measured CP and CC values is selected.

In Fig. 10 the CCPC is shown for the case where six predicted clutter covariances or PCCs are used. These PCCs were derived assuming three SAPs and two PCPs. The SAPs were shifted to -7[o] (cell 118 on the range bin), 0[o] (128.5) and 7[o] (139) from boresight and the PCPs were 57 and 75 dBs. The CCPC consists of CP and CC processors where their input is given by the waveform $\{ {}_{f}^{X}\sigma_{c,i}^2 \}$ and ${}_{f}^{X}\sigma_{c,i}^2$ denotes the i[th] front clutter source cell power corresponding to three different cases for X. They are:

1. X=UCMD when the clutter emanates from the storage uncompressed clutter memory device (UCMD) of Fig. 6.

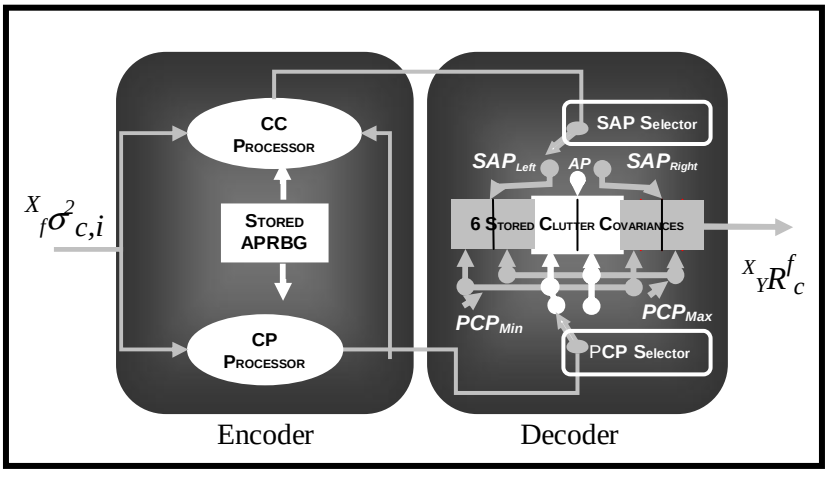

Fig. 10 Clutter Covariance Processor Compressor (CCPC)

2. X=RBCC when the clutter is generated from the radar-blind clutter coder of Fig. 7.
3. X=RSCC when the clutter is derived from the radar-seeing clutter coder of Fig. 8.

After the CP and CC values are determined on-line the CCPC selects from the memory containing the 6 PCCs of Fig. 10 the one that is better matched to the measured CC and CP processor output values. For instance, if the CC processor output is 140, the selection process is narrowed down to the pair of PCCs that were evaluated using the SAP that is shifted to position 139 on the range bin (or $+7^o$), since it is the closest. In addition, if the measured CP processor output is 60 dBs the element of the selected PCC pair associated with the 75 dB PCP is selected. Notice that the PCP_j selected is the one "above" the measured CP processor output value.

At this point two observations are made. The first is that the CC and CP Processors of Fig. 10 govern the 'on-line' time delay associated with the CCPC and constitute a 'lossy processor encoder' since they encode in a lossy fashion the time delay essence, called in [6] the ectropy, of the original CCP. The name ectropy is coined from Greek roots with 'ec' meaning outside and 'tropy' meaning to look and together signifying to look outside from input to output of the signal processor for its delay essence or maximum latency. The second observation is that the look up memory section of Fig. 10 is a 'lossy processor decoder' since it reconstructs a highly lossy version of the output of the original CCP.

Three space-time processors or SPTs are now defined where the content of the UCMD is applied to three different types of CCPCs. The weighting vector **w** of the three STPs is defined as follows

$$\mathbf{w} = [{}^{UCMD}_{CCPC}R]^{-1}\mathbf{s} \tag{3.6}$$

$${}^{UCMD}_{CCPC}R = R\big|_{R_c^f = {}^{UCMD}_{CCPC}R_c^f} \tag{3.7}$$

$${}^{UCMD}_{CCPC}R_c^f \in \{PCC(k,j)\}\big|_{S^{UCMD}_{CCPC}} \tag{3.8}$$

where: a) $R\big|_{R_c^f = {}^{UCMD}_{CCPC}R_c^f}$ is the total disturbance covariance (2.11)-(2.12) with the CCPC output of Fig. 10, ${}^{UCMD}_{CCPC}R_c^f$, replacing the front clutter covariance matrix R_c^f in (2.12); and b) S^{UCMD}_{CCPC} is the set of UCMD and CCPC parameters that define the specific CCPC case.

3.4.1. CCPC Case I

This first CCPC Case I has only one PCC pair and does not use any SAP since $\theta^1 = 0^o$ which corresponds to the physically implemented antenna pattern of Fig. 1 which is directed towards boresight. The defining set S^{UCMD}_{CCPC} is then given by the following expression:

$$S^{UCMD}_{CCPC} = \{{}_f\,\sigma^2_{c,i}, \theta^1 = 0^o, PCP_1 = 57dBs, PCP_2 = 75dBs\} \tag{3.9}$$

3.4.2. CCPC Case II

This second CCPC Case II has three PCC pairs. One is associated with the antenna pattern of Fig. 1 and the other two with two different SAPs. The defining set S^{UCMD}_{CCPC} is given by the following expression:

$$S^{UCMD}_{CCPC} = \{{}_f\,\sigma^2_{c,i}, \theta^1 = -7^o, \theta^2 = 0^o, \theta^3 = 7^o, PCP_1 = 57dBs, PCP_2 = 75dBs\} \tag{3.10}$$

3.4.3. CCPC Case III

This third CCPC Case III has five PCC pairs. One is associated with the antenna pattern of Fig. 1 and the other four with four different SAPs. The defining set S^{UCMD}_{CCPC} is given by the following expression:

$$S^{UCMP}_{CCPC} = \{{}_f\,\sigma^2_{c,i}, \theta^1 = -14^o, \theta^2 = -7^o, \theta^3 = 0^o, \theta^4 = 7^o, \theta^5 = 14^o, PCP_1 = 57\,dBs, PCP_2 = 75dBs\} \tag{3.11}$$

In Fig. 11 the simulation results for range bin #1 of Fig. 4 is presented for the above three cases as well as the not knowledge-aided SPT sample matrix inverse (SMI) scheme defined below

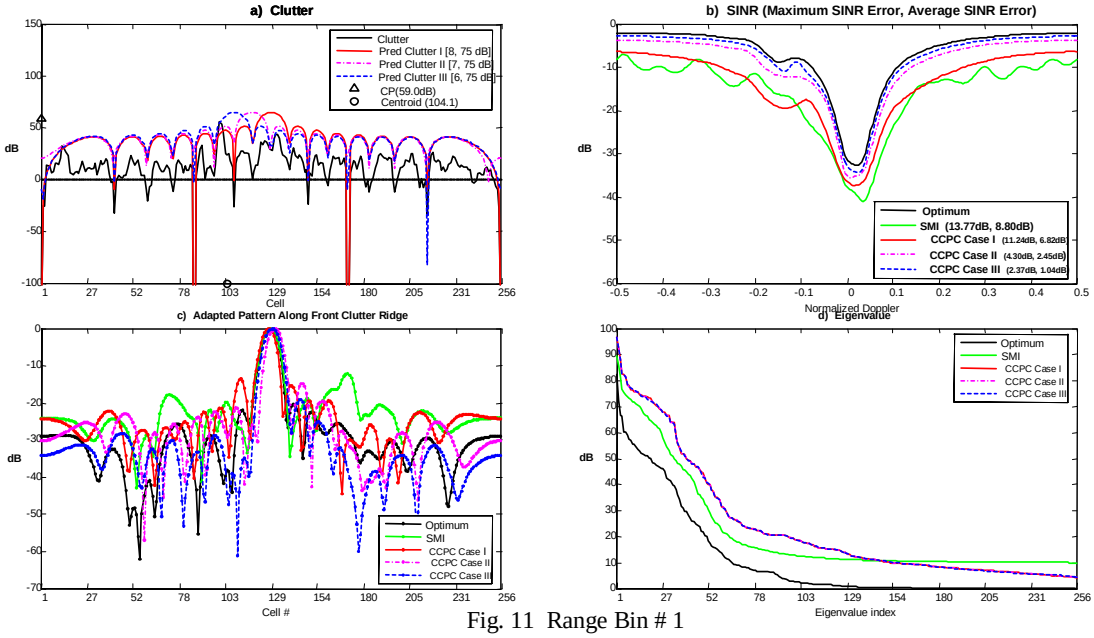

Fig. 11 Range Bin # 1

$$\mathbf{w} = [{}^{smi}R]^{-1}\mathbf{s} \tag{3.12}$$

$${}^{smi}R = \frac{1}{Lsmi}\sum_{i=1}^{Lsmi} X_i X_i^H + \sigma^2_{diag} I \tag{3.13}$$

where X_i denotes radar measurements from range bins close to the range bin under investigation, *Lsmi* is the number of measurement samples and $\sigma^2_{diag}I$ is a diagonal loading term. When performing our investigations X_i was derived via the following generating equation

$$X_i = R_i^{-1/2}\mathbf{x}_i \tag{3.14}$$

where: a) $\mathbf{x}_i$ is a zero mean, unity variance, NM dimensional complex random draw; and b) R_i is the total disturbance covariance (2.11)-(2.12) associated with the i[th] range bin. As in [2] $\sigma^2_{diag} = 10$ is assumed in the simulations. For the simulations results shown in Fig. 11 *Lsmi* = 512 corresponding to 8 passes of the 64 range bins SAR image of Fig. 4. In addition, the radar and environmental condition parameters assumed for all the simulations are similar to those used in the companion paper [2] and are given in Table 1 for ease of reference (note that no jammers are assumed in our simulations, however, it should also be kept in mind that outstanding SINR radar performance results are derived when there are jammers present). Fig. 11 is now explained in some detail. In Fig. 11a, the ideal front clutter power $p_C^f(\theta_c^i, \theta_t)$ of (2.15) is plotted versus the range bin cell position. Note from Fig. 1 that range bin cell position 1 corresponds to -90°, 128.5 to 0° and 256 to +90° where all the angles are measured from boresight. Furthermore, the power axis has been marked with the corresponding CP of 59 dB and the cell position axis with the corresponding CC of 104.1 which is also noted to reside 24.4 range bin cells away (-17.1°) from the assumed target location of 128.5 or 0°. The ideal clutter waveform is then contrasted with the predicted ones derived from (3.4) and linked to the selected PCC for each CCPC scheme. The legends shown on this figure are discussed next.

The discussion begins with the legend "Pred Clutter I (8,75.0dB)". Pred Clutter I pertains to the front predicted clutter cell power (3.4) for CCPC Case I. To understand the meaning of the ordered pair (8,75.0dB) Fig. 12 must be studied first. It presents the front antenna pattern of Fig. 1 plotted in more detail as a function of cell location for any range bin. From this figure it is noted that there are 15 lobes (since the assumed number of antenna elements is N=16, see Table 1) where lobe 8 corresponds to the main lobe. In addition, this figure is characterized by the following set of zero crossings and mainlobe peak positions across the range-bin:

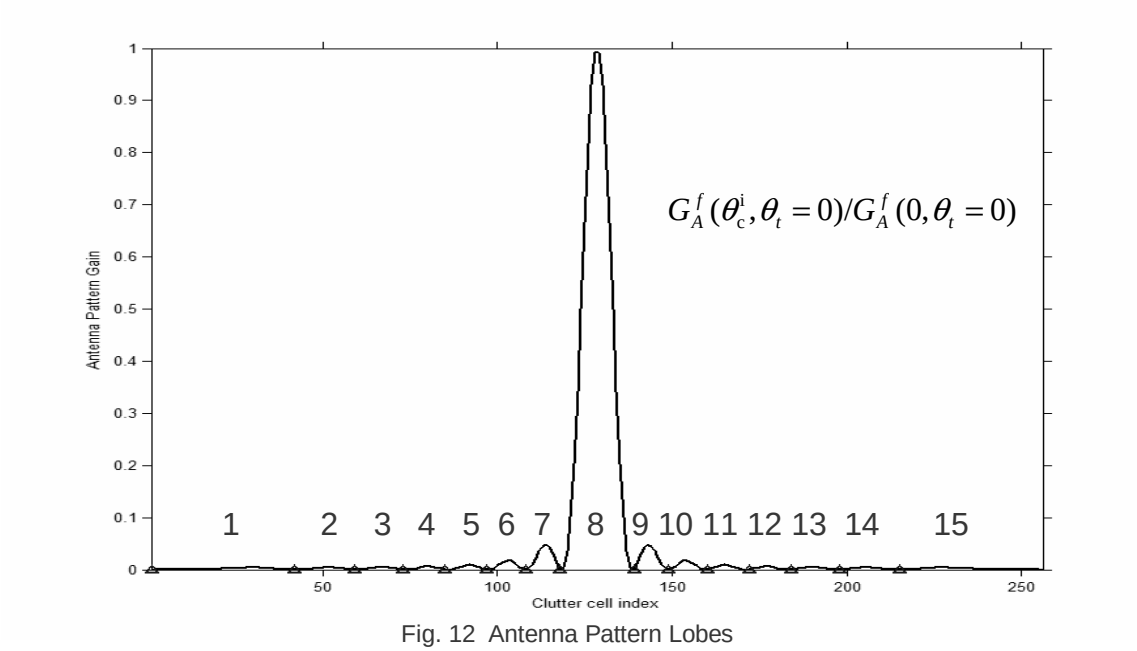

Fig. 12 Antenna Pattern Lobes

$$\begin{aligned} I &= [\ ZP^1, ZP^2, \ ZP^3, \ ZP^4, \ ZP^5, \ ZP^6, ZP^7, \ ZP^8, \ ZP^9, \ ZP^{10}, ZP^{11}, ZP^{12}, ZP^{13}, ZP^{14}, ZP^{15}] \\ &= [\ 42, \ 59, \ 73, \ 85, \ 97, \ 108, 118, 128.5, 139, 149, 160, \ 172, \ 184, \ 198, 215] \text{ cell position} \\ &= [-60.5,-48.5,-38.7,-30.2,-21.8, -14, \ -7, \ \ 0, \ \ 7, \ 14, \ 21.8, 30.2, 38.7, 48.5, 60.5] \text{ degrees} \end{aligned} \tag{3.15}$$

This set is then used to denote the possible directions to which the true antenna pattern of Fig. 1 can be shifted. Among these possible directions are those given in expressions (3.9)-(3.11) where SAPs are defined for three different CCPC cases. However, it is emphasized, that there is nothing magical about these directions since they can generally be anywhere in the specified range of cell locations from 1 to 256. In fact, numerous simulations have revealed outstanding SINR radar performance with directions that are anywhere in between the best two adjacent directions selected from (3.15). In other words, these directions have only been selected because they scan the entire range bin from cell 1 to cell 256 and have some connection to the lobes of the true antenna pattern. Clearly, the best placement for these positions is an open problem. The ordered pairs appearing in Fig. 11a can now be explained. For instance, the ordered pair (8,75.0dBs) next to the title Pred Clutter I inform us that the SAP associated with the selected PCC of CCPC Case I of (3.9) is the physically implemented antenna pattern of Fig. 12 where the predicted clutter power or PCP is 75.0 dBs. As a second example it is noted that the legend Pred Clutter II (7,75.0dBs) inform us that the plotted predicted clutter covariance power waveform corresponds to that of CCPC Case II of (3.10) where the antenna pattern had been shifted to -7^o away from boresight and the PCP is once again 75.0 dBs.

In Fig. 11b the SINR results derived with each scheme are presented. The title for each legend is self explanatory as well as the ordered pair consisting of the maximum SINR error followed by the average SINR error. Note how significantly better results are derived for CCPC Cases II and III than the SMI case and the CCPC Case I. Furthermore note that CCPC Case III outperforms CCPC Case II by a relatively small amount. In Fig. 11c the adapted pattern corresponding to all contrasted cases is plotted. The adapted pattern is defined as follows

$$AP(\theta_c^i, \theta_{AAM}, \beta, \theta_t, f_D^t) = 10\log_{10}\left|w^H \mathbf{c}^f(\theta_c^i, \theta_{AAM})\right|^2 \tag{3.16}$$

where $\theta_{AAM} = 2^o,\ \beta = 1,\ \theta_t = 0,\ \ f_D^t = 0$, $\mathbf{w}$ is given by either expression (3.6) or (3.12) and $\mathbf{c}^f(\theta_c^i, \theta_{AAM})$ by (2.17). Finally, in Fig. 11d the eigenvalues in dBs of the total disturbance covariance is plotted versus eigenvalue index for each case.

Next in Figs. 13 a & b the average and maximum SINR errors are plotted versus the 64 range bins of Fig. 4. The results presented in Fig. 13 correlate with those presented for range bin #1. In other words, it is concluded that CCPC Cases II and III (with average of average SINR error (AASE) values of 1.2 and 1.16, respectively) yield a satisfactory SINR performance while the SMI and CCPC Case I do not.

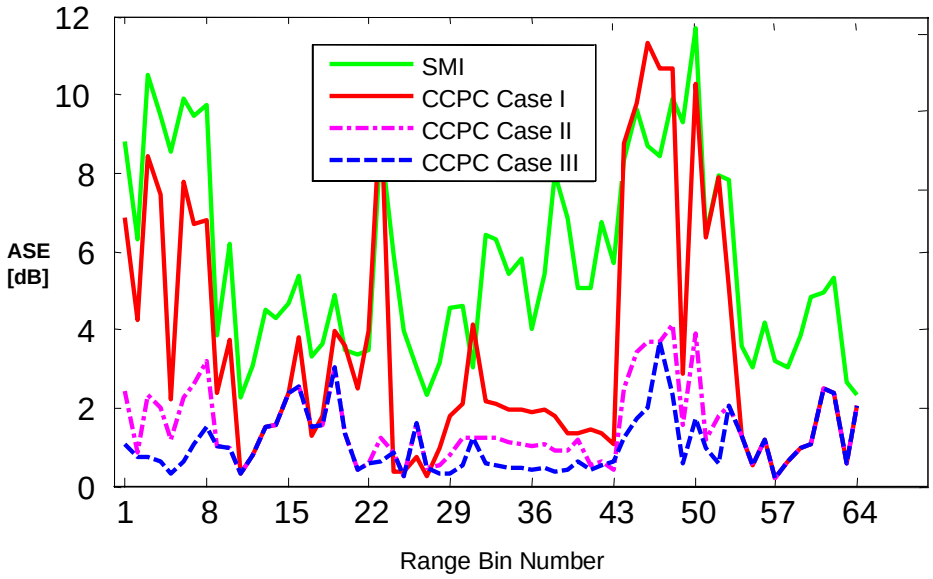

Fig. 13 a) Average SINR Error (ASE) versus Range Bin Number

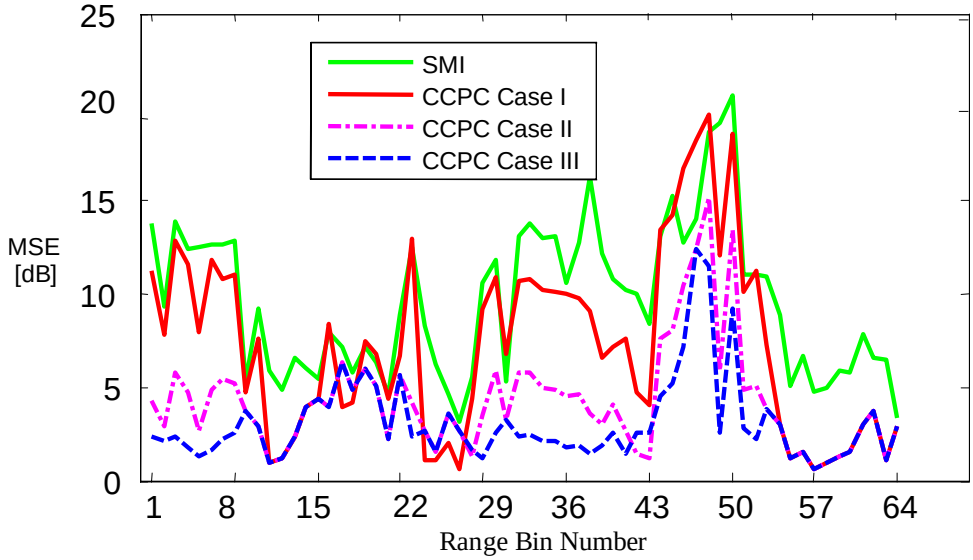

Fig. 13 b) Maximum SINR Error (MSE) versus Range Bin Number

3.5. Integrated Clutter Space Compressor and CCP Time Compressor

The results that are derived when the output of the RBCC of Fig. 7 is used in conjunction with CCPC Case III defined by (3.11) with ${}_{f}\sigma_{c,i}^{2}$ replaced with ${}_{f}^{RBCC}\sigma_{c,i}^{2}$ are now discussed. The RBCC is of the predictive-transform type [2]-[3] and compresses the SAR image from 4 MBs to 512 bytes. In Fig. 14 the corresponding 512 bytes radar-blind PT decompressed SAR image is shown.

In Fig. 15 the RBCC clutter cell power and predicted clutter power for CCPC Case III are plotted versus clutter cell number for range bin 1. In Fig. 16 the average SINR error is presented versus all the 64 range bins where the AASE

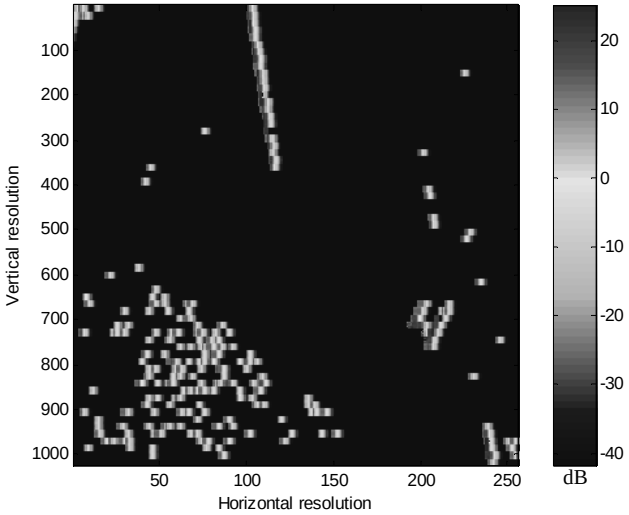

Fig. 14 512 Bytes PT Decompressed SAR Image

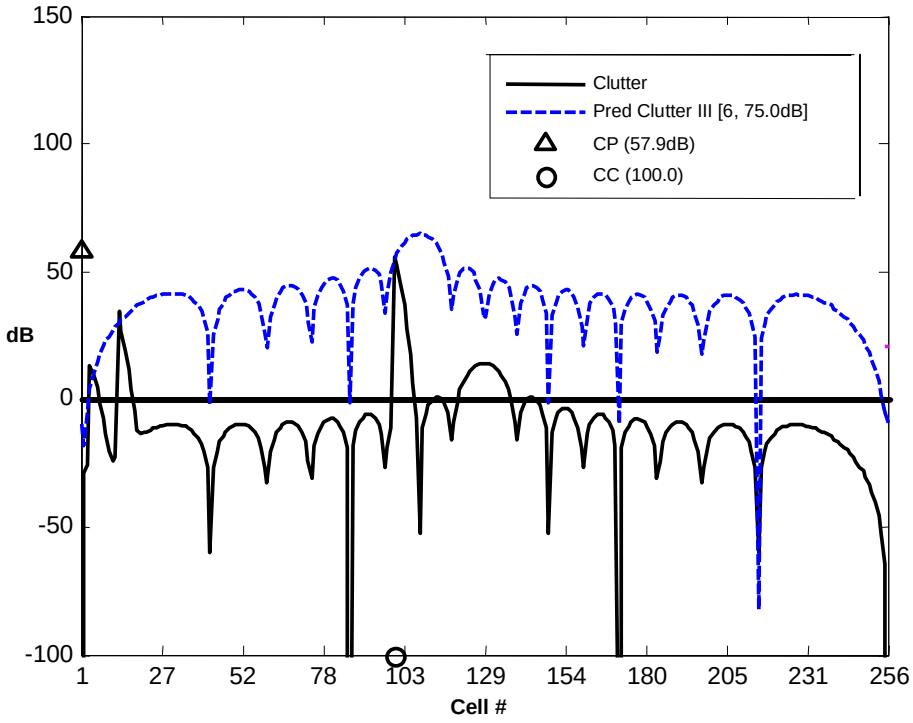

Fig. 15 Clutter Cell Power versus Cell # for Range Bin 1 and 512 Bytes RBCC

is given by 1.27 dBs. It should be noted that in the companion paper [2] it was found that when the straight CCP was implemented with the RBCC scheme it yielded an AASE value of 5.8 dBs. This result is surprising and not intuitive since the only way that a radar blind scheme has been found to perform adequately in KA-AMTI radar is when its straight CCP, which is obviously lossless, is replaced with a highly lossy CCPC.

Finally, it should be noted that when the radar seeing clutter coder or RSCC scheme with a compression ratio of 8,192 is combined with CCPC Case III the SINR results that are derived are close to those for the radar blind case. As a result the radar-blind scheme is preferred since besides being rather simple to implement it is a universal technique that can be embedded in any radar system.

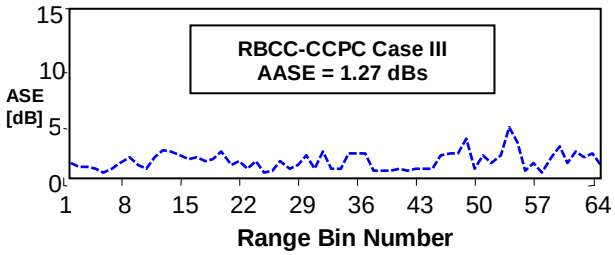

Fig. 16 Average SINR Error (ASE) versus Range Bin Number

Table 1. Simulation Parameter Values

a.	Antenna	N = 16, M = 16, d/λ = ½, $f_r = 10^3$ Hz, $f_c = 10^9$ Hz, $K^f = 4x10^5$ or 56 dBs, $K^b = 10^{-4}$ or -40 dBs,
b.	Clutter	N_c = 256, β = 1, 41 dBs < $10\log_{10}CP$ < 75 dBs, $_b\sigma^2_{c,i} = 1$ for all i, $10\log_{10}CP^b$ = -40 dBs,
c.	Target	$\theta_t = 0^o$
d.	Antenna Disturbance	$\sigma_n^2 = 1$, $\theta_{AAM} = 2^o$
f.	Range Walk	ρ = 0.999999
g.	Internal Clutter Motion	b = 5.7, $\omega = 15$ mph
h.	Narrowband CM	ε_i =0 for all i, γ_i for all i fluctuates with a 5^o rms
i.	Finite Bandwidth CM	$\Delta\varepsilon = 0.001$, $\Delta\phi = 0.1^o$
j.	Angle Dependent CM	$B = 10^8$ Hz, $\Delta\theta = 28.6^o$
k.	Sample Matrix Inverse	Lsmi = 8x64=512, $\sigma^2_{diag} = 10$.

4. CCPC ROBUSTNESS STUDY

In this section the robustness of the CCPC Case III of Section 3 is investigated by restricting the SAP mainlobe peak to reside at only one of the five positions $\{-14^o,-7^o,0^o,7^o,14^o\}$ specified in (3.11). This restriction leads to the following 'two PCCs' CCPC which is both simpler and faster than the original CCPC Case III:

$$\mathbf{w} = [{}^{RBCC}_{CCPC}R]^{-1}\mathbf{s} \tag{4.1}$$

$${}^{RBCC}_{CCPC}R = R\big|_{R_c^f = {}^{RBCC}_{CCPC}R_c^f} \tag{4.2}$$

$${}^{RBCC}_{CCPC}R_c^f \in \{PCC(k,j)\}\big|_{S^{RBCC}_{CCPC}} \tag{4.3}$$

$$S^{RBCC}_{CCPC} = \{{}^{RBCC}_{f}\sigma^2_{c,i}, \theta_{shift}, PCP_1 = 57dBs, PCP_2 = 75dBs\} \tag{4.4}$$

$$\theta_{shift} \in \{-14^o,-7^o,0^o,7^o,14^o\} \tag{4.5}$$

where the SAP mainlobe peak position θ_{shift} was tested for the five cases in (4.5) and the compressed/decompressed clutter source power ${}^{RBCC}_{f}\sigma^2_{c,i}$ was derived using a PT radar blind scheme [3]. When these five processor coders were simulated with the radar blind clutter compressor or RBCC the best AASE was produced when the SAP was shifted to either 14^o or -14^o. More specifically, the AASE values for these two cases emulated the value of 1.27 dBs shown in Fig. 16 for CCPC Case III. These results suggest that the simulated test SAR image is characterized by a 'pair' of SAPs symmetrically placed with respect to the moving target and where only one of them is needed for the CCPC to yield a satisfactory radar performance. An investigation of the clutter centroid plot of Fig. 9 further reveals that the best direction to shift the antenna pattern to over all 64 range bins may be governed by some power of the standard deviation of the clutter centroid from the boresight position (CC=128.5). It is of interest to note that when the clutter is homogeneous the clutter centroid will be equal to 128.5 for all 64 range bins and thus the selected SAP will point in the same direction as the 'actual' antenna pattern as expected [5].

Two natural consequences of our CCPC robustness study using the test SAR image are:

1. That for the considered test SAR image it is unnecessary to evaluate on-line the clutter centroid for each range bin since all that is needed is for us to determine 'off-line' the best global and symmetrically placed SAP pair to use with all range bins where only one of these SAPs is needed to construct the CCPC. Some preliminary investigations with an analytically tractable scalar example indicate that the reason why the SINR radar performance is relatively close when using either member of the symmetrically placed SAP pair is directly linked to the even/odd processing symmetries of the clutter steering vectors as well as the symmetrical structure of the antenna pattern.

2. That the 'off-line' determined best angle to shift our SAP to could be used to make the actual antenna pattern reflect this shifted position. A sample matrix inverse (SMI) technique can then be used with this 'physically build' SAP to yield a knowledge aided SMI scheme that can be viewed as an extreme case of memory space and computational time compressed KA-AMTI radar. The confirmation of this prediction for our test SAR image is summarized in Fig. 18 for which the following three observations are made:

   - The SINR expressions that were used to derive the SMI-AASE results are as follows:

$$SINR(\theta_{shift}) = \frac{\mathbf{w}(\theta_{shift})^t \mathbf{s}\mathbf{s}^t \mathbf{w}(\theta_{shift})}{\mathbf{w}(\theta_{shift})^t R(\theta_{shift}=0)\mathbf{w}(\theta_{shift})} \tag{4.6}$$

$$\mathbf{w}(\theta_{shift}) = [{}^{smi}R(\theta_{shift})]^{-1}\mathbf{s} \tag{4.7}$$

$${}^{smi}R(\theta_{shift}) = \frac{1}{Lsmi}\sum_{i=1}^{Lsmi} X_i(\theta_{shift}) X_i^H(\theta_{shift}) + \sigma^2_{diag} I \tag{4.8}$$

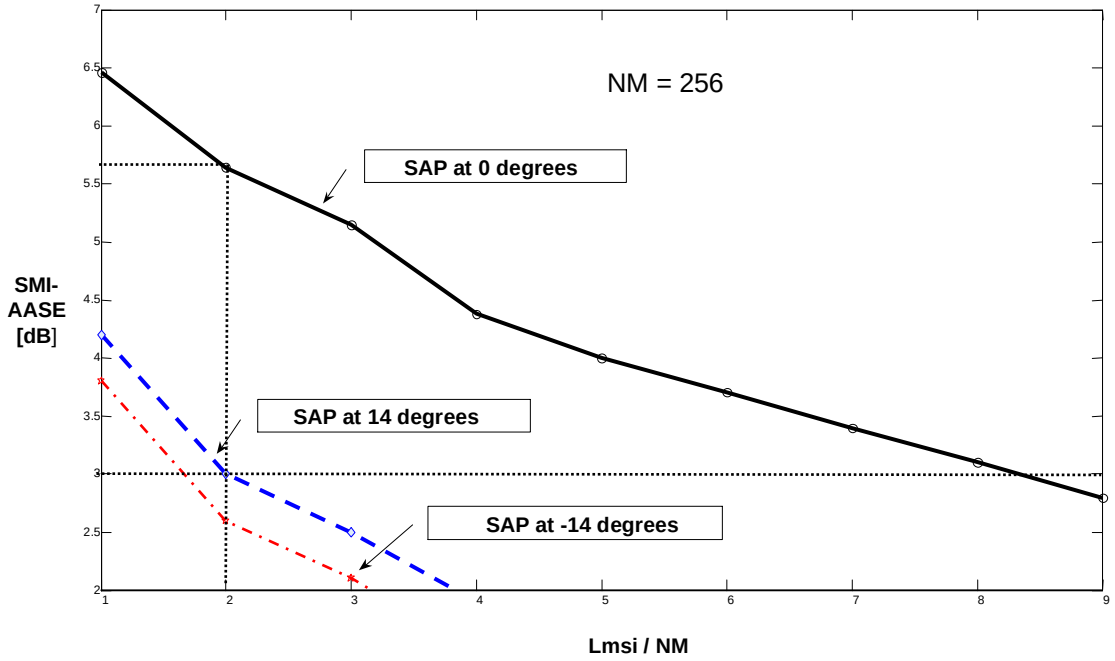

Fig. 18 SMI-AASE versus Lmsi/NM

$$X_i(\theta_{shift}) = R_i^{-1/2}(\theta_{shift})\mathbf{x}_i \tag{4.9}$$

$$R_i(\theta_{shift}) = R_i\big|_{G_A^f(\theta_c^t,\theta_t=0) \Rightarrow G_A^f(\theta_c^t-\theta_{shift},\theta_t=0)} \tag{4.10}$$

$$\theta_{shift} \in \{-14^o, 0^o, 14^o\} \tag{4.11}$$

where: a) $X_i(.)$ denotes a radar measurement from a range bin close to the range bin under investigation; b) L_{smi} is the number of measurement samples; c) $\sigma^2_{diag}I$ is a diagonal loading term where σ^2_{diag} = 10; d) $\mathbf{x}_i$ is a zero mean, unity variance, NM dimensional complex random draw; e) R_i is the total disturbance covariance (2.11)-(2.12) associated with the i[th] range bin; and f) θ_{shift} is the angle from boresight to where the peak of the antenna pattern has been shifted.

- It is noted that when the SAP is shifted to either +14 or -14 degrees from boresight a significantly better average of average SINR error (AASE) is derived confirming our predicted result that was inferred from our robustness study of the CCPC Case III.

- Of the three SAPs simulated the best result is derived when the SAP is shifted to -14^o from boresight. For instance, note how for *Lsmi* = 512 the derived AASE value of 2.6 dBs is at least 3 dBs better than the 5.7 dBs that is derived with the not knowledge aided SMI case when θ_{shift} = 0 degrees.

5. CONCLUSIONS

In this paper the SAR imagery clutter covariance processor appearing in KA-AMTI radar was replaced with a fast clutter covariance processor resulting in outstanding SINR radar performance while processing clutter that had been highly compressed using a predictive-transform radar blind scheme [3]. It was also noted that the advanced fast clutter covariance processor is a 'lossy' processor coder that can be viewed as the computational time compression dual of a 'lossy' source coder [6]. Since a significantly more complex radar seeing scheme did not noticeably improve the results derived with the radar blind case, it was concluded that the radar blind clutter compression method was preferred due to its simplicity and universal use with any type of radar system. This result was surprising since it was found earlier in a companion paper [2] that a radar blind scheme does not yield a satisfactory SINR radar performance when used together with a 'lossless' straight clutter covariance processor. In addition, since the fast clutter covariance processor output departed sharply from that of the significantly slower straight clutter covariance processor, it was established that when designing a fast clutter covariance processor for a radar application it was unnecessary to be concerned about how well the output of the fast processor matches that of the slower straight clutter covariance processor. This observation suggested a paradigm shift in fast signal processor design, where the emphasis before was in how well the fast signal processor output matched that of the slow original signal processor and now is in how well the fast signal processor impacts the overall system performance. A robustness study also revealed that the CCPC yielded outstanding SINR radar performance when only a single shifted antenna pattern was used in its construction. In turn this observation was used to study a simple knowledge aided sample matrix inverse (SMI) technique whose samples depended on clutter returns associated with a physically transmitted antenna pattern whose pointing direction was the same as that of the best SAP derived from our CCPC robustness study. This approach was found to yield a satisfactory SINR radar performance. In an appendix a novel predictive-transform sidelobe canceller was also advanced that achieved further reduced-dimension adaptivity [5] and was noted to significantly outperform principal components. In addition, as mentioned earlier in the conclusion section of [2], SAR imagery provides 2-D profiles which can be quite aspect dependent thus it is suggested that the techniques developed in this paper be extended to more advanced 3-D scenarios.

As final comments it is noted that the latest compression-designs developments will be posted in the near future under the CSI/CUNY website "feria.csi.cuny.edu". In addition, all four related papers appearing in this proceedings, i.e., papers [2], [3], [6] and this paper, summarize, polish and further extend the 'final report' results to be published this May 2006 for the DARPA/KASSPER Grant No. FA8750-04-1-0047 titled "A Predictive-Transform (PT) Compression Architecture and Methodology for KASSPER". In this final report only work performed up to September 30, 2005 is reported when the KASSPER program ended its standard DARPA four year funding cycle.

APPENDIX A

In this appendix a novel PT sidelobe canceller is stated that can be used for reduced-dimension adaptivity (RDA) [5]. This space-time processing (SPT) technique is defined by the following two equations:

$$\mathbf{w} = \mathbf{s} - B^H(\mathbf{s}) \left[B(\mathbf{s})\, R\, B^H(\mathbf{s}) \right]^{-1} B(\mathbf{s}) R\mathbf{s} \tag{A.1}$$

$$B(\mathbf{s}) = [0_{K\times 1} \quad I_K \quad 0_{K\times(NM-K-1)}][Diag(\mathbf{s})T_{APT}]^H \tag{A.2}$$

where: a) **w** is the STP's *NM* dimensional and generally complex weighting column vector; b) **s** is the steering column vector of the moving target (2.1); c) *R* is the total interference plus noise covariance matrix defined by (2.11) and (2.12); d) *Diag*(**s**) is a diagonal operator that produces a matrix of dimension *NM*x*NM* whose elements are all zero except for its diagonal elements which are the *NM* elements of **s**; e) T_{APT} is a real matrix of dimension *NM*x*NM* appropriately designed using either standard or accelerated predictive-transform (ATP) signal source modeling [3] where a special case of this matrix is the Karhunen-Loeve Transform (KLT), standard or accelerated; and f) $B(\mathbf{s})$ is a complex matrix of *K x NM* dimension where the value of *K* is noted from (A.1) to govern the order of the pre-requisite inversion of the expression $B(\mathbf{s})\, R\, B^H(\mathbf{s})$.

Two observations are made about the PT sidelobe canceller:

- When simulated with our test SAR image K = 31 is found to yield outstanding SINR radar performance. Furthermore, when the method of principal components was used with the same reduced dimension a very poor performance was derived. This result is not surprising, however, since the method of principal components depends on the rank of R and it is noted from Fig. 11d that this rank is significantly larger than 31.

- As noted from expression (A.2) the PT sidelobe canceller is signal dependent. However, its evaluation can be readily accelerated using parallelism [5].

REFERENCES

1. Guerci, J.R. and Baranoski, E, " Knowledge-Aided Adaptive Radar at DARPA", *IEEE Signal Processing Magazine*, vol. 23, no. 1, pp. 41-50, January 2006
2. Feria, E.H., "Compression-Designs of SAR Imagery Used as Prior Knowledge", *Proceedings of SPIE Defense and Security Symposium*, 17-21 April 2006
3. Feria, E. H. and Licul, D., "A Bit Planes Predictive-Transform Source Coder Illustrated with SAR Imagery", *Proceedings of SPIE Defense and Security Symposium*, 17-21 April 2006
4. Ward, J., Space-Time Adaptive Processing for Airborne Radar, MIT Technical Report 1015, *MIT Lincoln Laboratory*, December 1994
5. Guerci, J.R., " Space-Time Adaptive Processing for Radar", *Artech House*, 2003
6. Feria, E.H., "The Mathematical Theory of Signal Processing and Compression-Designs", *Proceedings of SPIE Defense and Security Symposium*, 17-21 April 2006
7. Shannon, C. E., "A Mathematical Theory of Communication", *The Bell System Technical Journal*, Vol. 27, pp. 379-423, 623-656, July, October, 1948

ACKNOWLEDGEMENTS

Dr. Joseph R. Guerci, the Director of DARPA's Special Projects Office (SPO), and Dr. Edward Baranoski, the Program Manager for DARPA's Knowledge-Aided Sensory Signal Processing Expert Reasoning (KASSPER), are gratefully acknowledged for their guidance during the course of this research. Their objective criticisms, advice and suggestions at every stage of this project are highly appreciated. Also my student, Mr. Dalibor Licul, whose expert programming and computer networking skills greatly facilitated this research and, for this, I am indebted to him.